Supplemental Figure 1

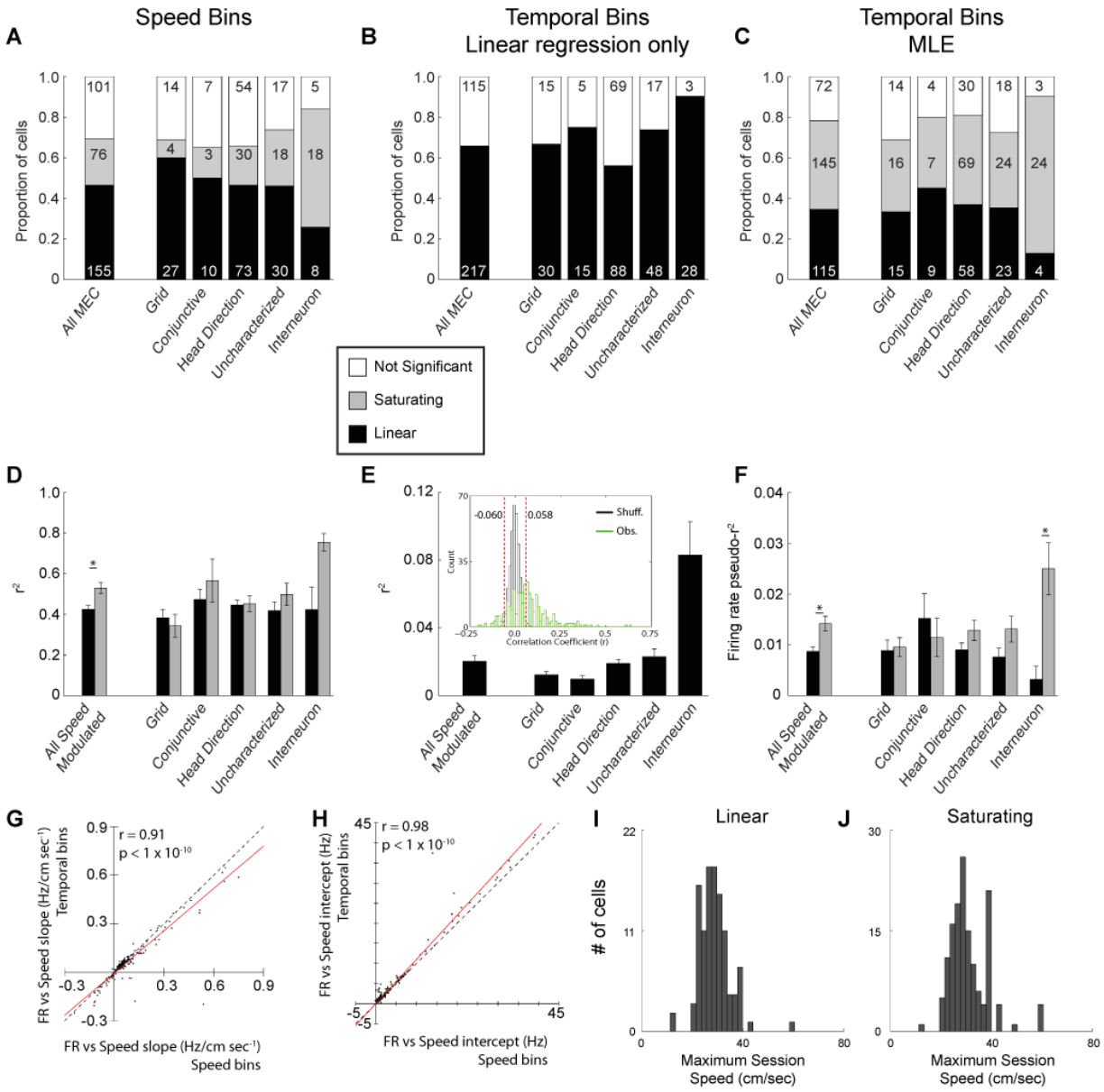

Figure S1. Related to Figure 1. Comparison of multiple approaches of identifying speed modulation. A) Binning data according to speed yields qualitatively similar proportions of speed modulated cells, although there is a tendency to overestimate the number of linearly speed coding cells. B) Performing a linear regression on temporally binned data and using a shuffling procedure to set a significance threshold identifies a qualitatively similar proportion of speed modulated cells, but by definition cannot identify non-linear firing rate to running speed relationships. C) Same plot as in Figure 1C shown again for comparative purposes. D) Mean +/- SEM r^2 values for the significantly speed modulated cells identified using the speed binned data. Note that this approach over estimates the amount of variance explained by running speed. E) Mean +/- SEM r2 values for the significantly speed modulated cells identified using temporal bins, linear regression and thresholds obtained through a shuffling procedure. The inset plot shows the distribution of shuffled correlation coefficients (black) with the counts normalized by the number of shuffles (100x per cell) and the distribution of observed correlation coefficients (green). Dashed red lines show the 1st and 99th percentile thresholds of the shuffled distribution. F) Same plot as in

Figure 1D shown again for comparative purposes. G) Scatter plot showing the similarity of the firing rate versus running speed slopes obtained using speed binned and temporally binned data. Red line shows regression line. H) Same as in G, but for the y-intercept. I) Distribution of maximum session running speed for cells identified as linear. J) Same as in *I*, but for cells identified as saturating.

Supplemental Figure 2

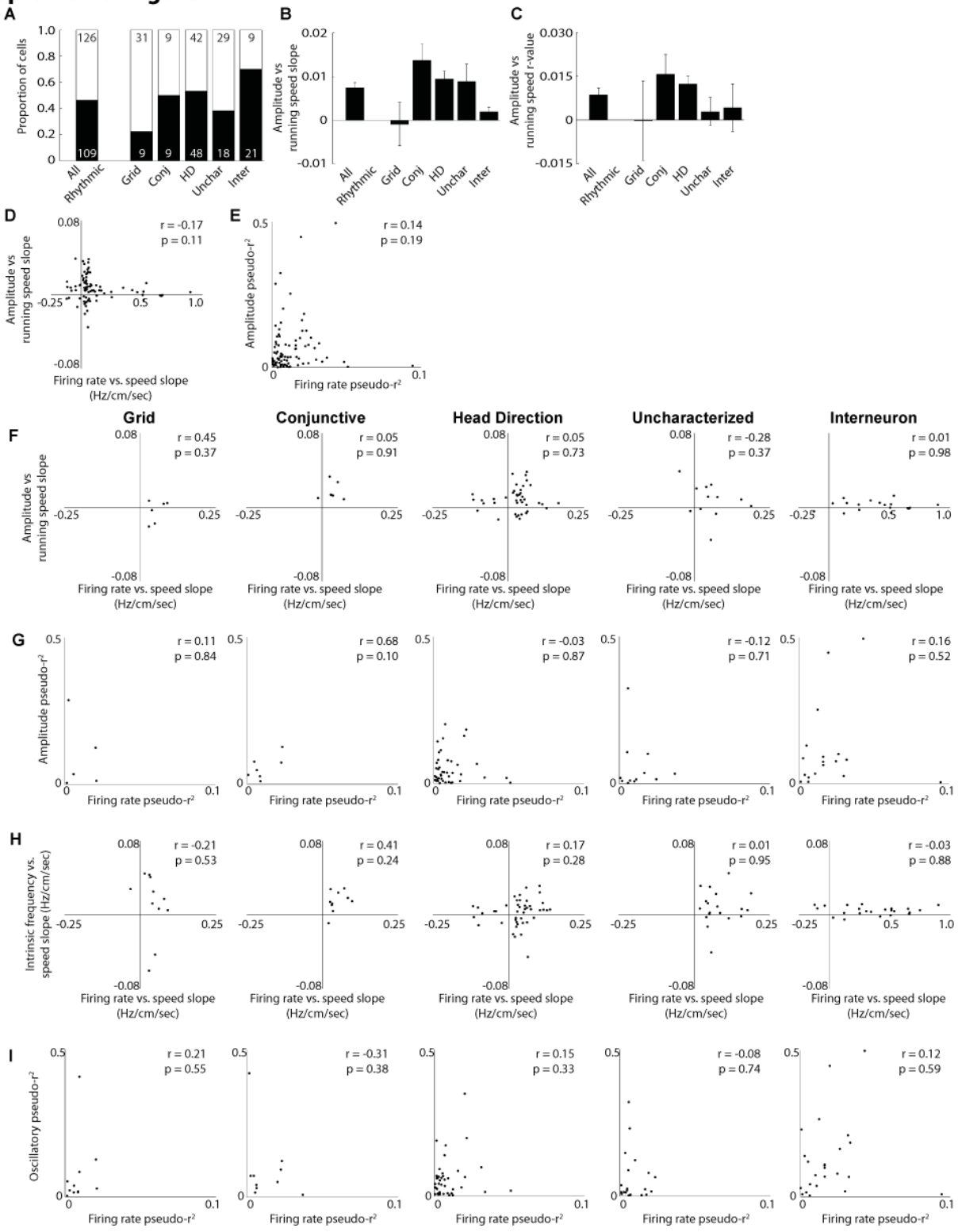

Figure S2. Related to Figure 3. A) Proportion of theta rhythmic cells with significant variation in the depth of theta modulation as a function of running speed. B) Mean +/- SEM slope of the relationship between the depth of theta modulation versus running speed. C) Mean +/- SEM r-value of the relationship between the depth of theta

modulation versus running speed. D) Scatterplot showing the lack of a relationship between slopes for firing rate versus running speed and depth of theta modulation versus running speed. E) Same as in D, but for the r-values. F) Data as in D broken down by cell type. G) Data as in E broken down by cell type. H) Data as in Figure 3I broken down by cell type. I) Data as in Figure 3J broken down by cell type.

Supplemental Figure 3

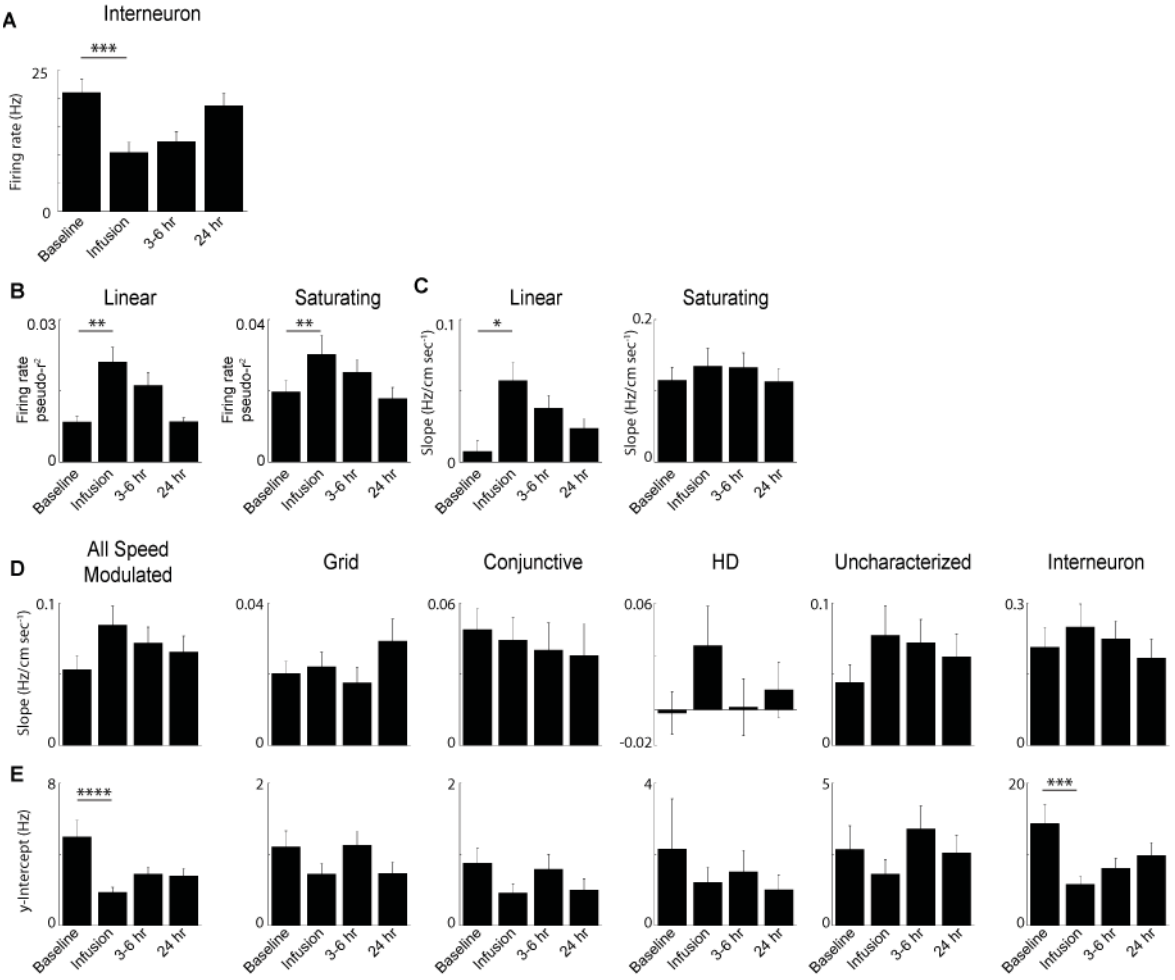

Figure S3. Related to Figure 5. A) Interneuron firing rates across Baseline, MS infusion and two recovery sessions. B) Firing rate versus running speed pseudo-r^2 values for Linear and Saturating cells during Baseline, MS infusion and two recovery sessions. C) Firing rate versus running speed slope values for Linear and Saturating cells during Baseline, MS infusion and two recovery sessions. D) Firing rate versus running speed slopes during Baseline, MS infusion and two recovery sessions. E) Same as B but for y-intercepts. * $p < 0.05$, ** $p < 0.01$, *** $p < 0.0005$, **** $p < 0.00005$

Supplemental Figure 4

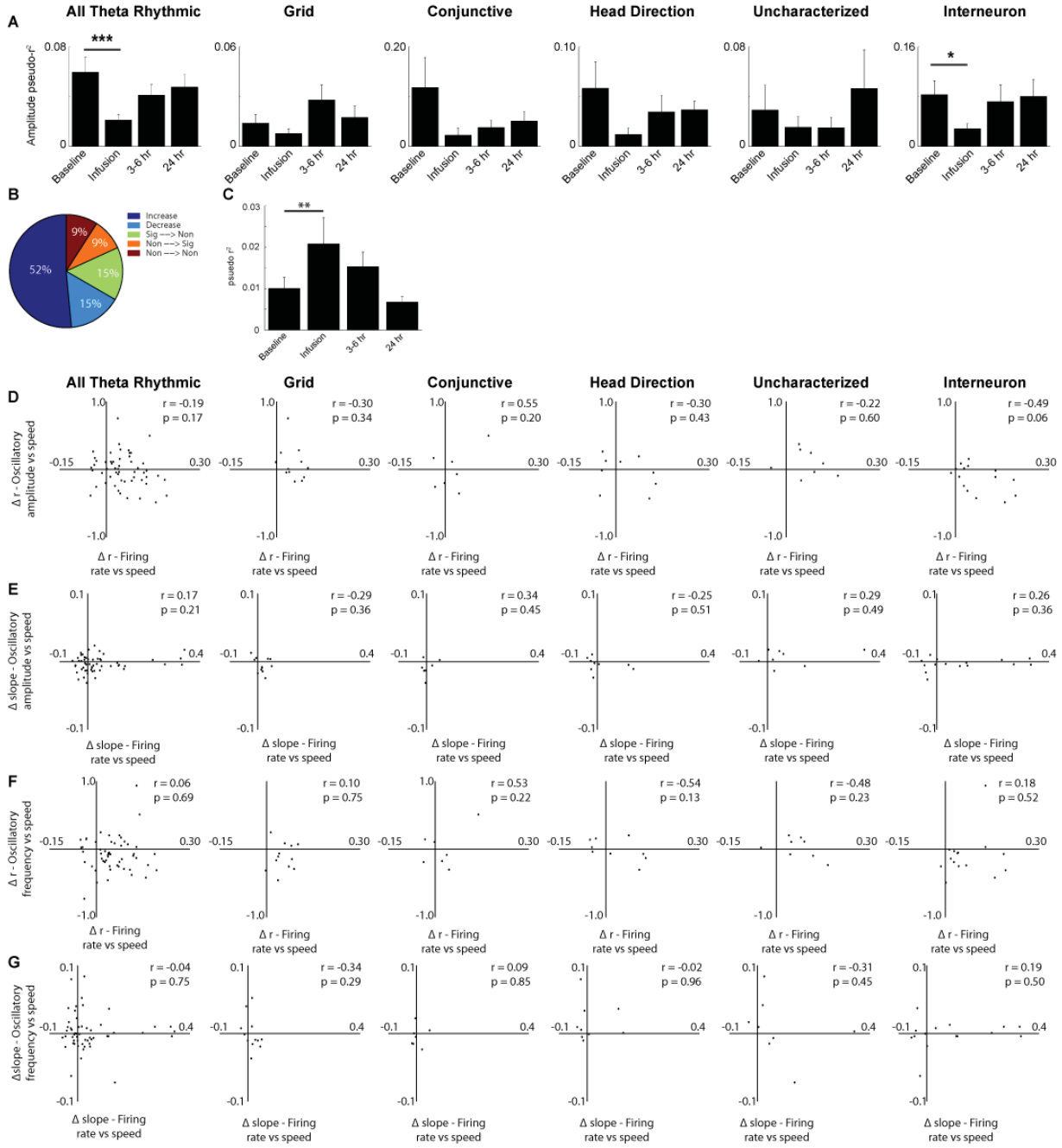

Figure S4 Related to Figure 6. A) Mean +/- SEM pseudo-r^2 of the relationship between depth of theta modulation and running speed for Baseline, MS infusion, 3-6 hour and 24 hour recovery sessions. B) Proportion of cells showing various changes in the strength of firing rate speed modulation among those cells that lost theta rhythmicity during MS infusion. C) Mean firing rate versus running speed pseudo-r^2 of the cells that lost theta rhythmicity during MS infusion. D) Scatterplots showing the lack of a relationship between the change in the r-values for firing rate versus running speed and depth of theta modulation versus running speed. E) Same as in D, but for the change in slope. F) Scatterplots showing the lack of a relationship between the change in r-values for firing rate versus running speed and oscillatory frequency versus running speed. G) Same as in F, but for the change in slope. * $p < 0.05$, ** $p < 0.005$, *** $p < 0.0005$

Supplemental Experimental Procedures

Subjects: This paper uses data gathered during experiments for which some results have previously been published (Brandon et al., 2011, 2013). Six adult male Long-Evans rats (500-650g) obtained from Charles River Labs (Wilmington, MA) were used. All animals were cared for using standard procedures that included individually housing them in plexiglass cages and maintaining them on a 12/12 hour light/dark cycle in a temperature and humidity controlled facility. All experimental procedures were approved by the Institutional Animal Care and Use Committee for the Charles River Campus at Boston University.

Presurgical Procedures: Prior to surgery animals were habituated to both the testing environment and being handled by experimenters. All animals were maintained at ~85% of their *ad libitum* weight in order to facilitate foraging for small pieces of Froot Loops (General Mills, Battle Creek, MI) in an open field environment (100 by 115 cm or 112 by 158 cm). Both open field environments contained a large white cue card on one wall and animals were familiarized with foraging for cereal pieces in the open field, as well as having contact with the experimenter.

Surgery: The surgical procedures have previously been described in detail (Brandon et al., 2011, 2013), but, briefly, a custom built hyperdrive housing 12 tetrodes aimed at dorsomedial entorhinal cortex and one or two infusion cannula directed at the medial septum were implanted. Atropine (0.04 mg/kg) was administered prior to induction of anesthesia. All surgical procedures were conducted under anesthesia induced with Isoflurane and a ketamine cocktail (Ketamine: 12.92 mg/kg, Acepromazine: 0.1 mg/kg, Xylazine: 1.31 mg/kg). Upon the loss of toe pinch reflex rats were placed in a stereotaxic frame, a midline incision was made in the skin above the skull and the skull was cleared of all connective tissue. Anchor screws were positioned across the skull surrounding the implant sites for the MS cannula (AP: +0.5 mm, ML: 2.0 mm, DV: 4.5 mm relative to bregma and penetrating the brain at a 20° angle) and the MEC hyperdrive (AP: -6.0 mm, ML: 4.5 mm relative to bregma). After lowering the cannula into the brain it was secured to the anchor screws with dental cement. Upon lowering the hyperdrive to the surface of the brain the remaining space in the skull hole was filled with silicone and then the hyperdrive was secured to the anchor screws with dental cement. A ground screw was positioned over the cerebellum. Once all of the implants were firmly secured in position, tetrodes were lowered 2 – 3 mm from the dorsal surface of the brain. After surgery animals were allowed to recover for seven days prior to any experimental involvement.

Behavioral testing and medial septal inactivation: All recordings were obtained while rats foraged for small pieces of Froot Loops in a large open field environment (100 by 115 cm or 112 by 158 cm) that had a large white cue card on one wall. Each recording session lasted 20 minutes. A subset of recording sessions involved pharmacological inactivations of MS with the $GABA_A$ agonist muscimol. A pre-infusion baseline recording session was conducted prior to any infusions that lasted 20 minutes. The protocol for muscimol infusions has been described previously (Brandon et al., 2011, 2013). The injector cannula was primed and inserted into the guide cannula where it extended 1mm beyond the end of the guide cannula. A total volume of 0.5 µL of muscimol diluted in phosphate-buffered saline was infused with a microinfusion pump (Harvard Aparatus, Holliston, MA) at a rate of 0.125 µL/min. At the

end of the four minute injection the infusion cannula was left in place for an additional two minutes to allow proper diffusion of the solution away from the injection site. After waiting 15 minutes from the end of the infusion, a post-infusion recording was begun that lasted up to 60 minutes. A recovery recording was conducted 3-6 hours after the infusion and an additional recovery session was attempted 24 hours after the infusion when cells could be stably held across days with each recording lasting 20 minutes.

Electrophysiological data acquisition: Electrophysiological recordings were obtained as rats foraged in an open field environment. All neural signals were pre-amplified on the headstage and subsequently transmitted to a Digital Lynx SX data acquisition system (Neuralynx, Bozeman, MT) where the signals were amplified (5,000 – 20,000X) and bandpass filtered (0.3-6 kHz.). Spikes were detected online as a threshold crossing on any of the four wires of a tetrode, at which point a window around the threshold crossing was digitized at 32 kHz and stored for later analysis. Position and head direction information of the rat was obtained via an overhead video camera that monitored two LEDs attached to the headstage.

Cell classification: The various functional cell types found in MEC were identified using established approaches. Ratemaps were generated by aligning spike time stamps to behavioral data such that each spike fell within a single frame of behavioral data. The firing rate within each spatial bin was calculated as the number of spikes occurring while the animal was in that spatial bin over the total amount of time spent within the bin. These normalized 2D histograms were smoothed by a two-dimensional 3cm Gaussian Kernel to generate the final ratemap. Gridness scores were calculated as published previously (Brandon et al., 2011). This method takes the two-dimensional autocorrelation of the rate map and draws a ring to encompass the six peaks nearest to the center of the autocorrelogram. The inner radius of this ring is defined as one half the minimum distance from the center of the autocorrelation to adjacent peaks. The outer radius was allowed to vary from the same size as the inner radius to the edge of the autocorrelation map. Gridness scores for each ring is defined as the difference between the lowest correlation of a rotation observed at 60 or 120 degrees of rotation and the highest correlation observed at 30, 90 or 150 degrees. The final gridness score for the cell session is then calculated as the maximum gridness score among all of the rings.

Consistent with previous approaches, HD cells were identified based on the Watson's U^2 score of their head directional tuning curves (Johnson et al., 2005). The Watsons's U^2 statistic was chosen over other scores (such as mean-resultant length) because it is non-parametric, requiring no binning of data points and making no assumptions that the tuning curve is unimodal.

Border cells show a higher firing rate along one or more boundaries of the environment, thus a border score was employed as in (Solstad et al., 2008). This border score is defined as:

$$\frac{Cm - Dm}{Cm + Dm}$$

Where Dm is the normalized mean distance from the location of a spike to the nearest wall and Cm is the proportion of pixels along a wall greater than 60% of the max spatial firing rate. While border cells were identified amongst

the recorded cells, the number was generally low and therefore summary data for border cells is not presented as is done for the other cell types.

Using the spatial firing property scores described above, each cell was assigned to a single functional cell type. Grid cells were identified as those cells with a gridness score greater than 0.34 and Watson's U^2 value less than 8, while conjunctive grid-by-head direction cells were those cells with a gridness score greater than 0.34 and a Watson's U^2 greater than 8. Head direction cells were classified as those cells having a Watson's U^2 score greater than or equal to 8, but not showing the spatial periodicity of grid cells. Border cells were defined based on a border score of 0.5 or greater while also not having any single field over 1/3 the size of the entire environment (Solstad et al., 2008), but very few cells met this criterion and thus they were not considered further. Putative interneurons were identified as those cells that did not meet any functional cell class criteria, had mean firing rates greater than 8 Hz and waveforms with peak-to-trough durations less than 0.275 ms in line with previously published reports (Buetfering et al., 2014; Mizuseki et al., 2009). Cells that did not meet any functional cell class criteria or the firing rate and waveform shape criteria for interneurons were designated as 'uncharacterized' cells.

Temporally binned firing rate versus running speed and MLE: Firing rate was fit using a maximum likelihood estimator. The instantaneous running speed was taken from the Kalman velocity, based on displacement in location between each recorded tracking sample (Fyhn et al, 2004). The number of spikes x occurring in each video frame (30Hz) was counted. Only frames with instantaneous velocity greater than 2 cm sec^{-1} and less than the 95th percentile of running speeds were considered, in order to avoid under sampled regions. The firing rate parameter (λ) was assumed to follow one of two functions of running speed:

Linear:

$$\hat{\lambda} = \hat{b} \cdot v + \hat{a}$$

Saturating exponential:

$$\hat{\lambda} = \hat{k} - \hat{m} \cdot e^{-\hat{q} \cdot v}$$

Using a Poisson link function, the underlying firing rate parameter was fit using the 'mle' function within the MATLAB statistics toolbox. The log-likelihood for each of these generating functions was calculated and used to determine the F-value and p-score of each fit compared to the uniform fit, as well as a nested comparison of the saturating exponential to linear functions. A shuffling procedure was used in order to generate a distribution of p-values resulting from fitting spikes that are decoupled from the behavior of the animal. Spikes were shuffled by adding an independent random delay to each spike time. Random delays were taken from a uniform distribution ranging from 30 seconds to the duration of the session minus 30 seconds. If the shuffled spike time was past the end of the session, then it was wrapped around to the beginning of the session. The result is an essentially random spike series that is decoupled both from the behavior of the animal and any temporal structure between spikes. For each shuffle the random data was fit with both the linear and saturating exponential functions as described above. This was repeated 100 times for each cell and a distribution of the p-values from all cells was generated separately for both fits. The 1st percentile of both distributions was identified, which fell at p = 0.005 for the linear fit and p =

0.0065 for the saturating exponential fit. A significance threshold was then conservatively set at a p-value of 0.001 for each F-test, thus ensuring that cells identified as being significantly speed modulated met a p-value threshold smaller than that of more than 99% of the shuffled distributions. Under the null hypothesis for the nested model, the F statistic should be distributed on $F_{3-2,n-3}$ where n is the number of frames observed.

Because the relative number of spikes counted in each frame is relatively variable due to their stochastic nature, we used a pseudo-R^2 as a goodness of fit measure. Pseudo-R^2 values were calculated by estimating the portion of the variance or residual sum of squares in the counts of spikes in each frame explained by the model not explained by a Poisson variability, or

Pseudo-$R^2 = \frac{RSS_{ModelExplained}}{RSS_{Total} - RSS_{Poisson}} = \frac{\left(Var(x) - \frac{1}{n}\sum_{i=1}^{n}\left(x_i - \hat{\lambda}\right)^2\right)}{Var(x) - \bar{x}}$

$Var(x)$ is the sample variance, $\hat{\lambda}$ is the instantaneous rate predicted by the fit, x_i is the i^{th} observed count of spikes in a single frame, and n is the number of observations. Thus, $Var(x) - \frac{1}{n}\sum_{i=1}^{n}\left(x_i - \hat{\lambda}\right)^2$ is the variance remaining after accounting for the fit. For a series of independent Poisson observations, the variance is the average rate. For n large, this can be approximated by the average count in each frame, or $\bar{x}$. Thus, $Var(x) - \bar{x}$ is the variance unexplained by a simple Poisson process.

Velocity binned firing rate versus running speed: The instantaneous running speed was taken as the Kalman velocity based on displacement in location between each recorded tracking sample (Fyhn et al, 2004). Running speed was sorted into 1 cm/s bins and only speed bins that had at least 3 seconds of data over the course of the behavioral session were included in further analysis, thus resulting in each session having slightly different maximum running speeds for this analysis. The firing rate as a function of running speed for each cell was calculated as the number of spikes in each 1 cm/s bin of running speed divided by the total time spent in that speed bin. Confidence intervals for each speed bin were determined by the inverse pdf of the assumed underlying poisson. The firing rate of each cell as a function of running speed was fit with both a linear and saturating exponential function as above.

Temporally binned firing rate versus running speed and linear regression: The instantaneous firing rate was taken as the number of spikes in a videoframe, divided by the duration of the videoframe (0.33 seconds), and smoothed with a Gaussian filter with \sigma of 33ms and width of 330ms. This smoothed instantaneous firing rate was linearly correlated with the instantaneous velocity to give a Pearson-Correlation coefficient ([-1 1]). To determine critical values of this coefficient we shuffled each cell's spike times 100 times. Spikes were shuffled by adding an independent random delay to each spike time. Random delays were taken from a uniform distribution ranging from 30 seconds to the duration of the session minus the duration of the session. If the shuffled spike time was past the end of the session, then it was wrapped to the beginning of the session. The result is an essentially random spike series which is decoupled both from the behavior of the animal and any temporal structure between spikes. Cells were identified as speed modulated if the correlation coefficient was below the 1st percentile or greater than the 99th percentile of this shuffled distribution.

Rhythmic properties and covariation with speed: The properties of rhythmicity were examined using a variation of the maximum likelihood estimation approach (Climer et al., 2015), and the code is available at https://github.com/jrclimer/mle_rhythmicity. Briefly, a list of lags x_i was generated by finding all of the times a spike was found in a 2 second window following a spike, and subtracting the difference. A probability density function for these bins was defined as:

$$\mathcal{L}(x;\tau,b,c,f,s,r) = D\left((1-b)\exp\left(-\frac{x}{10^{\tau}}\right)\left(r\exp\left(-\frac{x}{10^{c}}\right)F(x) + 1\right)\right)\frac{\left(\left(2+2\sqrt{1-s}-s\right)\cos(2\pi f x)+4\,s\cos(\pi f x)+2-2\sqrt{1-s}-3s\right)}{4}$$

$$\frac{\left(\left(2+2\sqrt{1-s}-s\right)\cos(2\pi f x)+4\,s\cos(\pi f x)+2-2\sqrt{1-s}-3s\right)}{4}$$

Where $\mathcal{L}$ is the probability of a lag at time x, 10^{τ} is an overall exponential falloff rate caused by the animal leaving the high firing states of the neuron, b is a baseline, 10^{c} is an exponential falloff to the rhythmicity caused by variation in the frequency, f is the mean frequency of the modulation, s is the amount of theta cycle skipping between 0 and 1, r is the rhythmicity factor and D is a normalization factor such that $\int_{x=0}^{2}\mathcal{L}(x;\tau,b,c,f,s,r)=1$. The exponential falloff parameters τ and c measure the slow falloff in the number of spikes and the amplitude of the rhythm in autocorrelograms. For a more intuitive sense of these parameters, we encourage the reader to explore Dynamic Figure 1 from Climer et al 2015, available at http://bit.ly/1tJurco. We fit the data to this distribution by finding the maximum log likelihood, first by approximating the values using a particle swarm optimizer (Chen, 2014) and then using the *mle* function in MATLAB (MathWorks Natick, MA). To conditionalize the amplitude or frequency of the rhythmicity in the running speed of the animal, we first shifted the velocity to have zero mean. We then modeled τ, f and r as linearly varying with the running speed of the animal. We first estimated the full fit of the data using the *mle* function, first by holding the other values constant at the initial fit, and the other parameters with a zero slope and y-intercept from the initial fit. This gave estimated slopes and intercepts for τ, f and r. We then estimated the full fit using MLE from this point, giving intercepts (log10(sec), Hz, and unitless for τ, f and r) and slopes ($\frac{\log_{10} sec}{\frac{cm}{sec}}, \frac{Hz}{\frac{cm}{sec}}$, and $\frac{1}{\frac{cm}{sec}}$ respecitlvey). Significance was determided by comparing the maximum log likelihood to the maximum log likelihood when the parameters f or r were held constant. The slopes and y-intercept for the depth of modulation, a, were determined by scaling the terms for r by $(1-b)$. To plot the rhythmicity over the velocity, spikes were binned using 0.02 second time bins and 50 speed bins spanning 0 to the 99th percentile of speeds, occupancy normalized, and smoothed by a Gaussian kernel with a standard deviation of 1 bin.

We measured the goodness of the speed-modulated fits by the deviance of the speed modulated fit and the baseline rhythmic fit from a uniform fit, or:

Pseudo $R^2 = 1 - \frac{LL_{unif} - LL_A}{LL_{unif} - LL_0}$

Where $LL_{unif}, LL_A, and\ LL_0$ are the log-likelihoods of the uniform, speed-modulated, and baseline rhythmic fits respectively. This differs from the speed modulation of firing rates because we are comparing to the baseline rhythmic fit, rather than an overall constant rate. To determine the significance of these rhythmic fits we used a partial F test, comparing the log-likelihood of a uniform, non-speed modulated rhythmic, and speed modulated rhythmic distributions. The deviance between any two models was taken as twice the difference in the log-likelihood and compared to a chi squared distribution.

Theta phase locking: Local field potential theta signals were obtained by filtering the raw LFP data with a third order band pass Butterworth filter with a high pass value of 6 Hz and a low pass value of 10 Hz. The instantaneous theta phase and magnitude were calculated as the angle and magnitude of the Hilbert transform of the filtered theta signal, respectively. The preferred theta phase of firing and strength of theta phase locking of the spiking of each cell was calculated using the mean resultant angle (MRA) and length (MRL) respectively and were calculated as follows:

$$mra = atan2\big(imag(mean(e^{j\theta})), real(mean(e^{j\theta}))\big)$$

$$mrl = abs\big(mean(e^{j\theta})\big)$$

Where j is the imaginary constant, θ is the theta phase of each spike, atan2 is the four-quadrant arc tangent function, and imag() and real() represent the real and imaginary components of the complex exponential. Intuitively, this is equivalent to taking the mean of the sine and cosine separately. In order to ensure that changes in phase locking occurring as a function of speed were not the result of a different number of spikes occurring at different speeds a subsampling procedure was implemented. All subsampling was performed by finding the speed bin with the lowest number of spikes and permuting all other speed bins to have the same total number of spikes. Note that spikes in each bin were permuted, so that each spike could only be chosen once.

Linear-circular correlations: Linear-circular correlations (speed vs preferred phase) were performed as in previous reports (Kempter et al., 2012). Circular-linear slopes were found using the *fminsearch* function of MATLAB to minimize the error of:

$$R = \sqrt[2]{\left(\frac{1}{n}\sum_{i=1}^{n}\cos(\theta_i - sx_i)\right)^2 + \left(\frac{1}{n}\sum_{i=1}^{n}\sin(\theta_i - sx_i)\right)^2}$$

Where x is a sample of the linear variable, theta is a sample of the circular variable, s is the circular-linear slope and *i* is an index into the *n* samples of the variable. *fminsearch* finds the value of s which minimizes R.

Spikes per cycle and definition of cycle bounds: The Hilbert transform used in the rest of the methods places the beginning of a theta cycle (0°) at the peak of theta. However, for a subset of analyses (change in preferred phase as a function of running speed) we calculated the mean resultant angle of theta phase of spiking and subtracted half of

this from the phase of theta. After rewrapping the resulting phase vector to [0 2*pi] the result is that for all cells the preferred angle of spiking relative to this shifted theta phase is pi.

Statistics: Normality of distributions was not assumed, so comparisons were made using non-parametric statistics. Comparisons of single distributions for a difference from zero were performed using Wilcoxon sign-rank tests. For comparisons of two distributions Wilcoxon sign-rank or Wilcoxon rank-sum tests were used. The general approach taken was to perform the various statistical tests on the full set of relevant cells and then divide the cells into the different functional cell types and perform the same statistical test on each individual cell type.

Supplemental References

Brandon MP, Bogaard AR, Libby CP, Connerney MA, Gupta K, Hasselmo ME (2011) Reduction of theta rhythm dissociates grid cell spatial periodicity from directional tuning. *Science* 332(6029): 595-599.

Brandon MP, Bogaard AR, Schultheiss NW, Hasselmo ME (2013) Segregation of cortical head direction cell assemblies on alternating theta cycles. *Nat Neurosci* 16(6): 739-48.

Buetfering C, Allen K, Monyer H (2014) Parvalbumin interneurons provide grid cell-driven recurrent inhibition in the medial entorhinal cortex. *Nat Neurosci* 17(5): 710 – 718.

Chen SS. 2014. Another particle swarm toolbox. (http://www.mathworks.com/matlabcentral/fileexchange/25986), MATLAB Central File Exchange. Retrieved August 7, 2014.

Climer JR, Ditullio R, Newman EL, Hasselmo ME, Eden UT (2015) Examination of rhythmicity of extracellularly recorded neurons in the entorhinal cortex. *Hippocampus* 25(4): 460-473.Fyhn M, Molden S, Witter MP, Moser EI, Moser MB (2004) Spatial representation in the entorhinal cortex. *Science* 305(5688): 1258-1264.

Johnson A, Seeland K, Redish AD (2005) Reconstruction of the postsubiculum head direction signal from neural ensembles. *Hippocampus* 15(1): 86-96.

Kempter R, Leibold C, Buzsaki G, Diba K, Schmidt R (2012) Quantifying circular-linear associations: hippocampal phase precession. *J Neurosci Methods* 207(1): 113 – 124.

Mizuseki K, Sirota A, Pastalkova E, Buzsaki G (2009) Theta oscillations provide temporal windows for local circuit computation in the entorhinal-hippocampal loop. *Neuron* 64(2): 267-280.

Solstad T, Boccara CN, Kropff E, Moser MB, Moser EI (2008) Representation of geometric borders in the entorhinal cortex. *Science* 322(5909): 1865-1868.